J IRAN CHEM SOC (2015) 12:1431–1438
DOI 10.1007/s13738-015-0611-2

ORIGINAL PAPER

Sensitive determination of hydrogen peroxide based on a novel nonenzymatic electrochemical sensor: silver nanoparticles decorated on nanodiamonds

Biuck Habibi · Mojtaba Jahanbakhshi

Received: 30 September 2014 / Accepted: 17 February 2015 / Published online: 4 March 2015

Abstract In the present work, we report the fabrication and application of a sensitive nonenzymatic hydrogen peroxide (H_2O_2) sensor, using a nanocomposite, based on the nanodiamonds (NDs) decorated with silver nanoparticles (AgNPs/NDs). The AgNPs/NDs nanocomposite was prepared via a facile and efficient process. The field emission scanning electron microscopy, transmission electron microscopy, and X-ray diffraction were applied for characterization of the obtained nanocomposite. The electrochemical investigations have shown that the resulting AgNPs/NDs nanocomposite modified electrode has strong electrocatalytic activity toward H_2O_2 reduction which is attributed to the NDs that promoted the formation, uniform distribution, and electrocatalytic activity of the AgNPs. In the optimum conditions, the linear response range of the constructed H_2O_2 sensor was from 0.1 to 34.0 μM at applied potential of −0.2 V with a detection limit of 0.01 μM (S/N = 3). Also, the proposed sensor showed high sensitivity of 1.59×10^6 μAM^{-1} and was applied to measure the concentration of H_2O_2 in real samples. These results indicate that the AgNPs/NDs nanocomposite with high conductivity and stability has a promising potential in electrochemical sensors development.

Graphical abstract Electroreduction of H_2O_2 on the AgNPs/NDs/GCE.

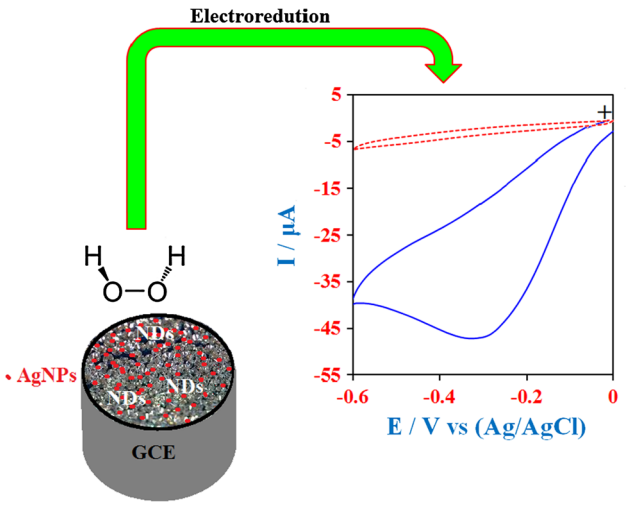

Keywords Nonenzymatic sensor · Electrocatalysis · Hydrogen peroxide · Silver nanoparticles · Nanodiamonds

Introduction

Detection of hydrogen peroxide (H_2O_2) has become extremely important in recent decades because of its wide and different applications and also its role as an important mediator in pharmaceutical, biological, clinical, industrial, and environmental investigations [1–3]. Numerous methods such as spectrophotometry [4], titrimetry [5], chemiluminescence [6], and chromatography [7] have been used in the determination of H_2O_2. However, the existing methods usually cannot offer high sensitivity, reliability, and operational simplicity at the same time, and often suffer from

Electronic supplementary material The online version of this article (doi:10.1007/s13738-015-0611-2) contains supplementary material, which is available to authorized users.

B. Habibi (✉) · M. Jahanbakhshi
Electroanalytical Chemistry Laboratory, Department of Chemistry, Faculty of Sciences, Azarbaijan Shahid Madani University, 53714-161 Tabriz, Iran
e-mail: B.Habibi@azaruniv.edu

interferences, time–cost, and use of expensive reagents [8]. Electrochemical methods, owing to their relatively low cost, high efficiency and sensitivity, and ease of operation, are suitable for the determination of H_2O_2, since they can achieve low detection limit and rapid response time on the basis of direct oxidation or reduction of H_2O_2 [9–13]. Electrochemical techniques, based on an enzyme or a protein, were also developed for the detection of H_2O_2 [14–18]. However, the enzymatic electroanalytical methods have some disadvantages such as complicated immobilization procedure, critical operating situation, instability, and high cost of enzymes [19, 20]. To overcome these problems, a number of studies have been carried out to improve the electrochemical response of H_2O_2 by the modification of the electrode surface without applying any enzyme or protein [9, 10, 12, 13, 21–24].

Nanostructured materials are attracting more and more attention due to their favorable performance in electrochemical sensors and biosensors. These materials, especially metal nanoparticles, can play an important role in improving of the nonenzymatic H_2O_2 sensors performance, owing to their large specific surface area, high electrocatalytic activity, and excellent conductivity. Contemporary investigations have demonstrated that silver nanoparticles (AgNPs) show favorable electrocatalytic activity for H_2O_2 reduction [10, 21, 23, 25–31]. The reported results in these works show that the electrocatalytic activity of the AgNPs is significantly related to their size and distribution. Also, in addition to the active metal itself, the AgNPs, the catalyst support plays a vital role in attaining electrocatalytic activity of the metal nanoparticles and consequently in the performance of the constructed sensors [25]. Carbon-based nanomaterials have attracted enormous attention as the ideal electrocatalyst supports due to their admirable and intrinsic properties [21, 23, 27, 32–36]. Among them, the nanodiamonds (NDs), the novel class of carbon nanomaterials that typically have carbon crystal cores with small size, low toxicity, high chemical stability, and ease of surface functionalization, have been widely examined [37–41]. So that, the cluster structure with a large specific surface area makes NDs as the suitable candidate for electrode materials in the construction of the electrochemical sensors and biosensors [41–44]. Consequently, to take full advantage of the NDs and AgNPs, it is desirable to produce a nanocomposite, based on silver nanoparticles and nanodiamonds (AgNPs/NDs), in which the NDs as support provide wide surface area over which the AgNPs can be highly dispersed and stabilized. This is essential for the catalysts to obtain good electrocatalytic activity and high permanence.

In the present work, for the first time, a nanocomposite of AgNPs and NDs was synthesized and characterized, using field emission scanning electron microscopy (FE-SEM), transmission electron microscopy (TEM), and X-ray diffraction (XRD). The obtained nanocomposite shows high electrocatalytic activity for the reduction of H_2O_2 and consequently is used for the fabrication of a non-enzymatic H_2O_2 sensor. Basically, by combining the advantages of the AgNPs and NDs, the prepared sensor exhibits its excellent performance toward H_2O_2 determination with high sensitivity, wide linear range, low detection limit, and excellent selectivity and reproducibility.

Experimental

Reagents

Nanodiamonds with average cluster size of 15 nm were purchased from plasma chem. Co. (Germany). $AgNO_3$ and H_2O_2 were obtained from Fluka (Sigma Aldrich). All other compounds were purchased from Fluka or Merck and were used without any additional purification. The 0.1-M phosphate buffer solution (PBS) pH 7.0 was applied as a supporting electrolyte. All of the solutions were prepared with double-distilled water.

Apparatus and measurements

The electrochemical measurements were carried out with AUTOLAB PGSTAT-100 (potentiostat/galvanostat). A three-electrode system with a platinum wire electrode, a silver/silver chloride electrode (Ag/AgCl, KCl 3 M), and an AgNPs/NDs modified glassy carbon electrode (AgNPs/NDs/GCE) was used, respectively, as the counter, the reference, and the working electrodes in the electrochemical experiments. A Bruker AXF (D8 Advance) X-ray power diffractometer was used for the XRD studies. The surface morphology and particle sizes of the AgNPs on the NDs were investigated by means of the field emission scanning electron microscopy on a JSM-6700F FE-SEM (JEOL Ltd., Japan) device through the operation of 15 kV and JEM-1200 EX/S transmission electron microscopy.

Preparation of the AgNPs/NDs/GCE

NDs were functionalized according to a standard procedure [45]. Briefly, 0.5 g of the NDs was heated first in a 9:1 (v/v) mixture of concentrated H_2SO_4 and HNO_3 at 75 °C for about 3 days, then in 0.1 M NaOH solution at 90 °C for 2 h, and afterward in 0.1 M HCl aqueous solution at 90 °C for another 2 h. The functionalized NDs (carboxylated) were separated by sedimentation using a centrifuge at 8000 rpm and widely rinsed with double-distilled water, and then dried in room temperature. 100 mL of the diluted

NDs suspension (with 0.2 wt%) was mixed with 100 mL of 0.01 M$AgNO_3$ solution for 2 h and then certain volumes of 0.2 M sodium borohydride ($NaBH_4$) was added to the obtained solution in the stirring condition, and at last it was further stirred at room temperature for 24 h until the Ag precursor was completely reduced. Afterward, the resultant nanocomposite was isolated by centrifuging and then rinsed by multiple washing steps using double-distilled water and finally dispersed in 10 mL double-distilled water by ultrasonication for about 60 min. For the preparation of nanocomposite modified GCE, 5 μL of AgNPs/NDs dispersed solution was directly placed on a carefully polished and washed GCE and dried at room temperature. For the comparison, AgNPs/MWCNTs/GCE was also prepared by the same process.

Results and discussion

The AgNPs/NDs nanocomposite characterization

FE-SEM is often used to observe the surface morphology of nanocomposite modified electrodes. On the other hand, particle size and distribution of metal nanoparticles on the supporter could be studied by TEM. FE-SEM image in Fig. 1a presents the nanocluster form of nanodiamonds particles on the GCE surface. Also, the others FE-SEM show high dispersion of the AgNPs on the NDs in the shape of a uniform film with cluster mold (Fig. 1b, c). Moreover, as can be seen in TEM image (Fig. 1d), the AgNPs on the cluster of the NDs have uniform distribution with average particle size of about 5–10 nm.

Phase, purity, and also presence of the AgNPs on the NDs were examined by XRD investigations. The XRD patterns of AgNPs/NDs and NDs powder are shown in Fig. 2 and its inset, respectively. The three peaks (inset of Fig. 2) at 43.90°, 75.4°, and 91.64° 2θ characterize the distinct diffraction peaks agreeing to form (111), (220), and (311) structure of NDs powder [46, 47]. The XRD pattern of AgNPs/NDs shows a shift in the position of the peaks of NDs which proves the presence of effective retraction between the AgNPs and the NDs (Fig. 2). Also the diffraction peaks of the AgNPs and the face-centered cubic phase of silver have good accordances with that of the AgNPs (111), (200), (220), and (311) planes. The presence of these peaks confirms that the AgNPs have been decorated on

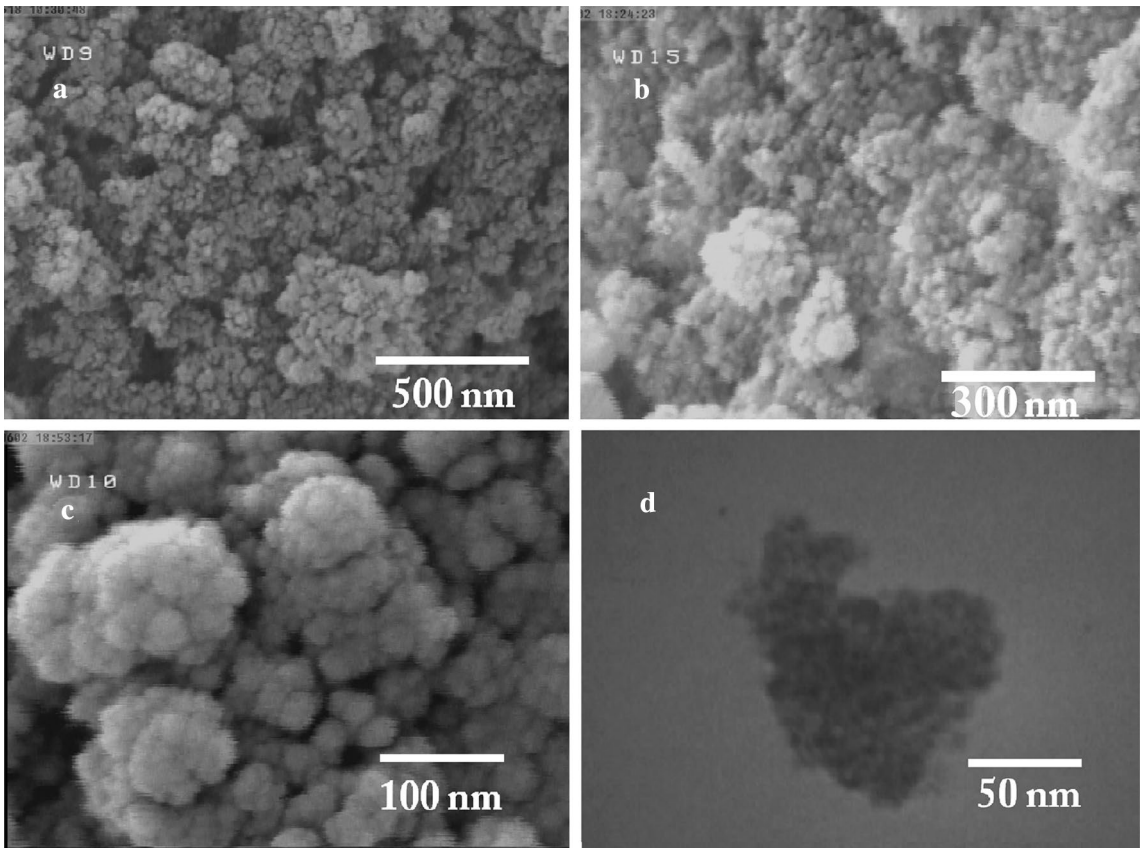

Fig. 1 **a** FE-SEM image of the NDs/GCE, (**b**, **c**) FE-SEM image of the AgNPs/NDs/GCE at low and high magnification, respectively, and (**d**) TEM image of the AgNPs/NDs

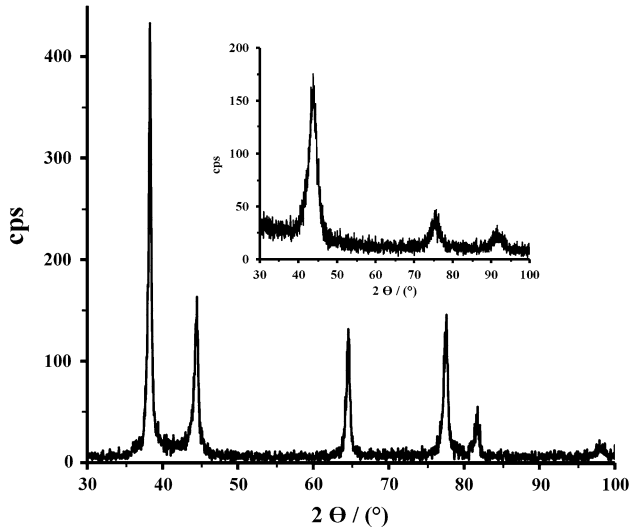

Fig. 2 XRD patterns of the AgNPs/NDs and NDs (inset)

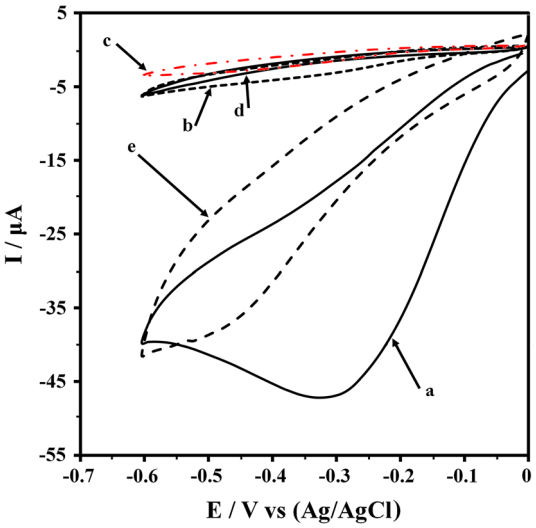

Fig. 3 Cyclic voltammograms of the AgNPs/NDs/GCE (*a*, *b*), with and without 0.1 mM H_2O_2, respectively, bare GCE (*c*), NDs/GCE (*d*), and AgNPs/MWCNTs/GCE (*e*) in PBS, pH 7.0 in the presence of 0.1 mM H_2O_2. Scan rate is 100 mVs^{-1}

the surface of the NDs. The XRD patterns in Fig. 2 and its inset are matched to the JCPDS file [48]. The absence of any characteristic peak in the XRD pattern of AgNPs/NDs indicates that the obtained nanocomposite has high purity.

Direct electrocatalysis and amperometric determination of H_2O_2

The electrochemical techniques such as cyclic voltammetry (CV) and chronoamperometery were used to establish the capability and electrocatalytic performance of AgNPs/NDs/GCE toward H_2O_2 reduction. The comparative investigation of the electrochemical response of different electrodes for H_2O_2 reduction is shown in Fig. 3. Curve a in Fig. 3 shows the electrocatalytic response of AgNPs/NDs/GCE toward the reduction of 0.1 mM H_2O_2 in PBS, pH 7.0. In the presence of H_2O_2, AgNPs/NDs/GCE shows a notable electrocatalytic response to H_2O_2 reduction with a peak current about 28 μA, which took place at about −0.30 V vs Ag/AgCl. On the other hand, curve b shows the response of AgNPs/NDs/GCE in the absence of H_2O_2. As shown, there is not any notable reduction peak on it and only a small background current was observed at the AgNPs/NDs/GCE in the absence of H_2O_2. Therefore, the response of AgNPs/NDs/GCE in the presence of 0.1 mM H_2O_2 (curve a) not only has a cathodic peak originated from the reduction of H_2O_2, but also has sufficient intensity for the determination of H_2O_2. Curves c and d in Fig. 3 show the responses of the bare GCE and NDs/GCE in the presence of 0.1 mM H_2O_2, respectively. As can be seen, in the studied potential region, small background currents are observed at the bare GCE and also at the NDs/GCE: the electrochemical responses of both of the electrodes are almost the same, which indicates that NDs/GCE similar to the bare GCE has no electrocatalytic activity toward H_2O_2 reduction. These results indicate that AgNPs/NDs/GCE possesses remarkable electrocatalytic ability toward H_2O_2 reduction, and the catalytic current mainly results from the presence of the AgNPs in the nanocomposite modified electrode. Furthermore, to illuminate the supporting effect of the NDs in the electrocatalytic activity of the AgNPs, with respect to the other conventional carbon nanomaterials, such as multi-walled carbon nanotubes (MWCNTs), the electrochemical activity of AgNPs/NDs/GCE was compared with that of a GCE, modified with AgNPs/MWCNTs (AgNPs/MWCNTs/GCE). Curve e in Fig. 3 shows the electrocatalytic response of the AgNPs/MWCNTs/GCE to the reduction of H_2O_2 in PBS, pH 7.0. The comparison of curves e and a shows that the reduction peak current of 0.1 M H_2O_2 at AgNPs/NDs/GCE (about 28 μA) is remarkably larger than (about three times) that of the AgNPs/MWCNTs/GCE (about 10 μA) and the cathodic overpotential for the reduction of H_2O_2 at AgNPs/NDs/GCE is obviously reduced by about 160 mV in comparison with that of the AgNPs/MWCNTs/GCE. Increasing the reduction peak current and decreasing overpotential can be attributed to the enhancement of electrocatalysis of the H_2O_2 reduction reaction [49], which arises from smaller size and higher surface area of the AgNPs on the surface of the NDs. Basically, the main role of the NDs with network-like structure as a support is providing a high surface area over which the AgNPs can be highly dispersed and stabilized. This feature is essential for the catalysts to obtain a large active area to contact with H_2O_2, good catalytic activity, and high performance and permanence. On the other

hand, these observations show that the AgNPs decorated on the NDs display prominent electrocatalytic performance toward H_2O_2 reduction, or high electrocatalytic H_2O_2 reduction peak current can be attributed to the presence of a large quantity of the AgNPs on the surface of the nanocomposite modified electrode.

According to the earlier studies [26, 50], the electroreduction mechanism of H_2O_2 on the AgNPs/NDs modified electrode can be illustrated by the following equations:

$$H_2O_2 + e^- \rightarrow OH_{(ads)} + OH^- \quad (1)$$

$$H_2O_2 + H^+ + OH_{(ads)} + e^- \rightarrow 2OH_{(ads)} + H_2O \quad (2)$$

In the first step, reduction of the primary H_2O_2 molecules provides the initial source of $OH_{(ads)}$ at a small overpotential, which in turn allows the reduction of the secondary H_2O_2 molecules at the higher rate. The activated process also results in the accumulation of $OH_{(ads)}$ intermediates on the nanocomposite modified electrode surface, provided that the reduction of H_2O_2 takes place continuously and increases the cathodic current as a result of the electrocatalytic activity of the AgNPs/NDs modified electrode. Consequently, the high electrocatalytic property of AgNPs/NDs toward the reduction of H_2O_2 results from the presence of the AgNPs which shows high electrocatalytic peak current for H_2O_2 reduction. As we know, the electrocatalytic property of the AgNPs is size-dependent and the small-sized Ag particles can lead to higher catalytic ability for decomposing H_2O_2 molecules [27]. As can be found in Fig. 1 c and d, the AgNPs were less agglomerated and uniformly distributed on the NDs. Meanwhile, the functionalized NDs effectively enhanced the conductivity of the nanocomposite modified electrode, so that the network-like structure could load a great amount of the AgNPs, facilitate the electron transfer for the reduction reaction, and provide large active surface area to contact with H_2O_2.

Another examination was performed to realize the transport features of H_2O_2 to the obtained nanocomposite modified electrode surface. For this purpose, the effect of the scan rate on the reduction reaction of H_2O_2 at the resulting sensor was studied by CV and shown in Fig. 4. As can be seen, the reduction currents increased with increasing the scan rates from 10 to 180 mV/s. The plot of H_2O_2 reduction peak current versus the square root of the scan rate shows a straight line (inset of Fig. 4), indicating that this process is controlled by H_2O_2 diffusion, which is an ideal route for the quantitative determinations [51].

For amperometric determination of H_2O_2, the prepared nanocomposite modified electrode is evaluated by measuring the current response at a fixed potential under a suitable pH value with the addition of H_2O_2. Figure 5 illustrates the typical current–time plot of AgNPs/NDs/GCE in PBS, pH 7.0, on continual addition of H_2O_2

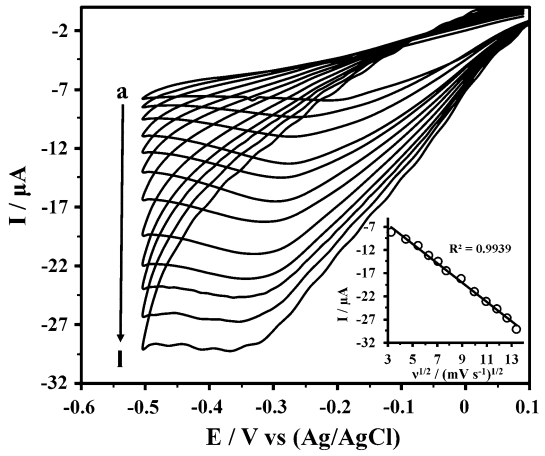

Fig. 4 Cyclic voltammograms of 0.05 mM H_2O_2 on the AgNPs/NDs/GCE at different scan rates in PBS, pH 7.0, *Curves a* to *l* corresponds to 10, 20, 30, 40, 50, 60, 80, 100, 120, 140, 160 and 180 mVs^{-1}, respectively. *Inset* is the plot of peak current versus square root of scan rate

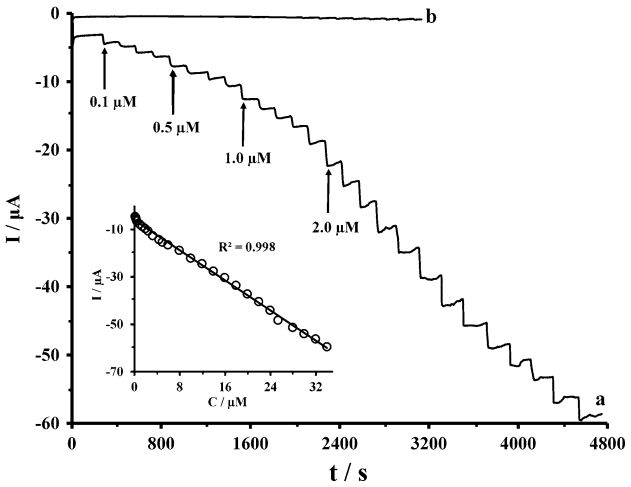

Fig. 5 Amperometric responses of the AgNPs/NDs/GCE to successive addition of H_2O_2 (*a*) and for NDs/GCE (*b*) in PBS, pH 7.0, under the conditions of −0.2 V constant potential and rotation speed of 1000 rpm. *Inset* is the plot of amperometric current vs. H_2O_2 concentration

concentrations. The resultant sensor showed a rapid and sensitive response to H_2O_2 concentration variation. Moreover, to further confirm that the electrocatalytic activity of AgNPs/NDs/GCE toward the H_2O_2 reduction arises from the presence of the AgNPs, we compared the response of the AgNPs/NDs/GCE (Fig. 5 curve a) with that of NDs/GCE (Fig. 5 curve b) for the same amount of H_2O_2. At the NDs-modified electrode, very low currents can be perceived (Fig. 5b), while the reduction currents for AgNPs/NDs/GCE (Fig. 5a) were considerably greater due to the high electrocatalytic performance of the AgNPs as well as the synergistic reinforcement of AgNPs/NDs. The

Table 1 Analytical performance of different H_2O_2 sensors based on the AgNPs

Sensor	Dynamic range	Limit of detection (μM)	Sensitivity (μAM^{-1})	Ref.
Ag/X-CPE	20 μM–11.76 mM	9.1	41.26×10^3	[9]
AgNPs/Ox-pTTBA/MWCNT	10–260 μM	0.24	2.42×10^6	[10]
SWCNT/AgNPs	0.01–8.0 mM	0.2	3.23×10^3	[23]
Pt/PVA/Ag	1.25 μM–1.0 mM	1.0	128.45×10^3	[24]
MWCNT/Ag	0.05–17 mM	0.05	1.42×10^3	[27]
AgNP-PPyCs/GCE	0.1–90 mM	1.05	–	[28]
AgNPs/ATP/GCE	10.0 μM–21.53 mM	2.4	–	[30]
MWNTs/Cu/Ag/GCE	2–420 μM	2.82	–	[50]
AgPs/SWCNT/PET	16 μM–18.085 mM	2.76	10.92×10^3	[51]
AgNPs/NDs/GCE	0.1–34 μM	0.01	1.59×10^6	This work

obtained linear range for the H_2O_2 concentrations on the AgNPs/NDs/GCE was about 0.1–34.0 μM ($R^2 = 0.998$) and the limit of detection and sensitivity were calculated to be 0.01 μM (S/N = 3) and $1.59 \times 10^6\,\mu AM^{-1}$, respectively. Comparison of the linear range, detection limit, and sensitivity of the present AgNPs/NDs modified electrode with other AgNPs based H_2O_2 sensors reported in the literature was shown in Table 1. All data in Table 1 reveal that the analytical performances of AgNPs/NDs/GCE are comparable with and even better than those obtained at the other AgNPs modified electrodes. Therefore, the AgNPs/NDs nanocomposite could be used for the preparation of a good performance amperometric H_2O_2 sensor with prompt response and wide linear range. On the other hand, compared to the enzymatic modified electrodes [21, 22], the present sensor not only does not lose its activity over time but also does not have the disadvantages of the enzymatic sensors such as complicated immobilization procedure and critical operating situation.

Sensor reproducibility, repeatability, and stability

The reproducibility, repeatability, and stability of a constructed sensor are essential for practical applications. Therefore, the reproducibility of the AgNPs/NDs/GCE was determined in 10 μM H_2O_2 solution through five evaluations. The obtained relative standard deviation (RSD) was about 2.3 %. Similarly, to estimate the repeatability of the prepared sensor, four independent modified electrodes were applied to determine 10 μM H_2O_2 and the calculated RSD was about 3.2 %, which reveals an excellent repeatability for the electrode preparation procedure. Moreover, the stability of the selected sensor was examined as follows: after recording the reduction peak current of 10 μM H_2O_2 at the optimum conditions, the sensor was washed with double-distilled water and kept in PBS, pH 7.0. It was found that the response value for 10 μM H_2O_2 reduced about 2.0 % in a week and about 6.0 % in a month. These results prove high stability and notable repeatability and reproducibility of the planned sensor.

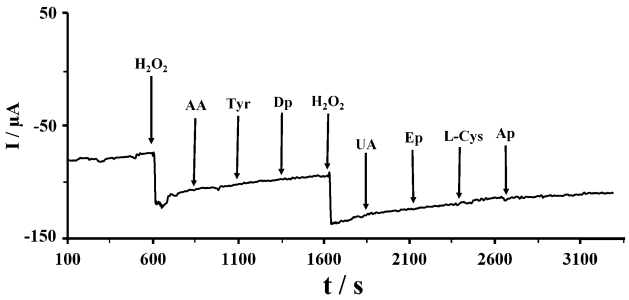

Fig. 6 Current-time *curve* for interfering effect of 0.1 mM AA, Tyr, D_P, UA, Ep, L-Cys, and Ap on the performance of the AgNPs/NDs/GCE in the sensing of 0.05 mM H_2O_2. Other conditions are the same as shown in Fig. 5

Anti-interference studies and real sample analysis

Anti-interference property is an important factor for the electrochemical sensors. Since the detection of H_2O_2 is an important task in many biological, medical, and clinical studies, the interferences of some electroactive compounds, which are commonly present in these samples, can prevent us from accurate determination of H_2O_2 concentration. In order to investigate the anti-interference property of the present nanocomposite modified electrode, the interference effects were examined by challenging the amperometric responses of some electroactive species such as ascorbic acid (AA), tyrosine (Tyr), dopamine (Dp), uric acid (UA), epinephrine (Ep), L-cysteine (L-Cys), and acetaminophen (Ap) on the AgNPs/NDs modified electrode in PBS, pH 7.0 at a working potential of −0.2 V, and in the presence of H_2O_2 (0.05 mM). The amperometric response of the present sensor for 0.1 mM of each above mentioned compounds and also 0.05 mM H_2O_2 is shown in Fig. 6. As can be seen in Fig. 6, successive addition of each interfering

species brought out hardly noticeable current response, but at the same time it show a well-defined H_2O_2 response for every addition of it. These results indicate that the present sensor has high selectivity in the H_2O_2 determination. Good anti-interference and high selective ability of the present sensor is generally attributed to the low working potential of −0.2 V used in the determination of H_2O_2.

Finally, in order to verify the reliability of the AgNPs/NDs/GCE sensor, the analysis of the real samples was performed by the determination of H_2O_2 concentration in the commercial eye drops. The mean value of H_2O_2 concentration in the eye drops samples was detected using two different methods: the present method (via constructed sensor) and the $KMnO_4$ titration method. As recorded in Table 2, the obtained mean values by the present sensor are near to the results which were determined by $KMnO_4$ titration technique and there is no significant difference between them [50]. This indicates that it is feasible to use the developed sensor for determining H_2O_2 in real samples. The above obtained results propose that the developed sensor is reliable and operative in determining H_2O_2 in medical or industrial samples.

Conclusions

In the present paper, a new sensitive method is established for the amperometric determination of H_2O_2 based on the decoration of the AgNPs on NDs by a facile and efficient procedure. Due to high surface area and network structure, NDs are ideal template for preparing the AgNPs nanocomposite. The results of electrochemical experiments indicate that the AgNPs were able to electrocatalyse the H_2O_2 reduction reaction. Consequently, the AgNPs/NDs nanocomposite was successfully applied to the fabrication of a novel nonenzymatic H_2O_2 sensor. At an applied potential of −0.2 V, the designed sensor has the detection limit of 0.01 μM, response concentration range from 0.1 to 34.0 μM, and sensitivity of 1.59×10^6 μAM^{-1}. This sensor was applied to measure the concentration of H_2O_2 in the eye drops samples. Therefore, due to the favorable electrocatalytic ability and analytical performances of the present sensor including high sensitivity and selectivity, low detection limit, prompt response, wide linearity range, long-term stability, repeatability, and reproducibility, the AgNPs/NDs nanocomposite is very promising for the future development of nonenzymatic H_2O_2 sensors.

Table 2 Determination of H_2O_2 in eyedrops samples by the developed method (AgNPs/NDs/GCE sensor) and titration method

Sample no.	This method (μM)	RSD[a] (%)	Titration method (μM)	RSD[a] (%)
1	9.0	3.0	8.8	3.1
2	18.0	3.5	17.7	2.9

[a] Number of sample assayed = 5

Acknowledgments The authors are grateful to the Research Office of Azarbaijan Shahid Madani University (Grant No. 214/d/10802), Tabriz, Iran for financial support.

References

1. M.V. Marshall, L.P. Cancro, S.L. Fischman, J. Periodontol. **66**, 786 (1995)
2. P.N. Bartlett, P.R. Birkin, J.H. Wang, F. Palmisano, G.D. Benedetto, Anal. Chem. **70**, 3685 (1998)
3. V. Patel, M. Kelleher, M. McGurk, Br. Dent. J. **23**, 61 (2010)
4. P.A. Tanner, A.Y.S. Wong, Anal. Chim. Acta **370**, 279 (1998)
5. N.V. Klassen, D. Marchington, H.C.E. McGowan, Anal. Chem. **66**, 2921 (1994)
6. T.C. Carmine, G. Bruchelt, T. Hahn, D. Niethammer, J. Biolumin, Chemilumin. **9**, 267 (1994)
7. U. Pinkernell, S. Effkemann, U. Karst, Anal. Chem. **69**, 3623 (1997)
8. W. Oungpipat, P.W. Alexander, P. Southwell-Keely, Anal. Chim. Acta **309**, 35 (1995)
9. S.N. Azizi, S. Ghasemi, S. Kavian, Biosens. Bioelectron. **62**, 1 (2014)
10. A.A. Abdelwahab, Y.-B. Shim, Sens. Actuat. B Chem. **201**, 51 (2014)
11. Y. Tang, Y. Guo, L. Zhang, J. Cai, P. Yang, Biosens. Bioelectron. **54**, 628 (2014)
12. C. Zhang, M. Wang, L. Liu, X. Yang, X. Xu, Electrochem. Commun. **33**, 131 (2013)
13. X. Li, X. Du, Z. Wang, X. Hao, G. Guan, H. Zhang, A. Abuliti, G. Ma, J. Electroanal. Chem. **717–718**, 69 (2014)
14. N. Jia, Q. Lian, Z. Wang, H. Shen, Sens. Actuat. B Chem. **137**, 230 (2009)
15. H. Qi, C. Zhang, X. Li, Sens. Actuat. B Chem. **114**, 364 (2006)
16. W.L. Zhu, Y. Zhou, J.R. Zhang, Talanta **80**, 224 (2009)
17. Q. Sheng, M. Wang, J. Zheng, Sens. Actuat. B Chem. **160**, 1070 (2011)
18. K. Szot, M.J. Niedziolka, E. Rozniecka, F. Marken, M. Opallo, Electrochim. Acta **89**, 132 (2013)
19. X. Miao, R. Yuan, Y. Chai, Y. Shi, Y. Yuan, J. Electroanal. Chem. **612**, 157 (2008)
20. V.G. Gavalas, N.A. Chaniotakis, Anal. Chim. Acta **404**, 67 (2000)
21. B. Habibi, M. Jahanbakhshi, Sens. Actuat. B Chem. **203**, 919 (2014)
22. B. Xu, M.L. Ye, Y.X. Yu, W.D. Zhang, Anal. Chim. Acta **674**, 20 (2010)
23. B. Habibi, M. Jahanbakhshi, M.H. Pournaghi-Azar, Microchim. Acta. **177**, 185 (2012)
24. M.R. Guascito, E. Filippo, C. Malitesta, D. Manno, A. Serra, A. Turco, Biosens. Bioelectron. **24**, 1057 (2008)
25. D. Li, L. Luo, Z. Pang, X. Chen, Y. Cai, Q. Wei, RSC Adv. **4**, 3857 (2014)
26. F.W. Campbell, S.R. Belding, R. Baron, L. Xiao, R.G. Compton, J. Phys. Chem. C **113**, 9053 (2009)
27. W. Zhao, H. Wang, X. Qin, X. Wang, Z. Zhao, Z. Miao, L. Chen, M. Shan, Y. Fang, Q. Chen, Talanta **80**, 1029 (2009)
28. X. Qin, W. Lu, Y. Luo, G. Chang, X. Sun, Electrochem. Commun. **13**, 785 (2011)

29. Y. Jiang, B. Zheng, J. Du, G. Liu, Y. Guo, D. Xiao, Talanta **112**, 129 (2013)
30. H. Chen, Z. Zhang, D. Cai, S. Zhang, B. Zhang, J. Tang, Z. Wu, Talanta **86**, 266 (2011)
31. S. Palanisamy, C. Karuppiah, S.M. Chen, R. Emmanuel, P. Muthukrishnan, P. Prakash, Sens. Actuat. B Chem. **202**, 177 (2014)
32. X. Li, Y. Liu, L. Zheng, M. Dong, Z. Xue, X. Lu, X. Liu, Electrochim. Acta **113**, 170 (2013)
33. W. Wu, S. Yang, S. Zhang, H. Zhang, C. Jiang, J. Colloid Interf. Sci. **427**, 15 (2014)
34. Y. Peng, L. Qiu, C. Pan, C. Wang, S. Shang, F. Yan, Electrochim. Acta **75**, 399 (2012)
35. B. Habibi, M. Jahanbakhshi, Electrochim. Acta **118**, 10 (2014)
36. X. Chen, K. Eckhard, M. Zhou, M. Bron, W. Schuhmann, Anal. Chem. **81**, 7597 (2009)
37. M. Singh, M. Holzinger, O. Biloivan, S. Cosnier, Carbon **61**, 349 (2013)
38. A.P. Puzyr, A.V. Baron, K.V. Purtov, E.V. Bortnikov, N.N. Skobelev, O.A. Mogilnaya, V.S. Bondar, Diam. Relat. Mater. **16**, 2124 (2007)
39. A.M. Schrand, L. Dai, J.J. Schlager, S.M. Hussain, E. Osawa, Diam. Relat. Mater. **16**, 2118 (2007)
40. J. Zang, Y. Wang, L. Bian, J. Zhang, F. Meng, Y. Zhao, S. Ren, X. Qu, Electrochim. Acta **72**, 68 (2012)
41. L.C.L. Huang, H.C. Chang, Langmuir **20**, 5879 (2004)
42. A.I. Gopalan, S. Komathi, G.S. Anand, K.P. Lee, Biosens. Bioelectron. **46**, 136 (2013)
43. L. Chen, J. Zang, Y. Wang, L. Bian, Electrochim. Acta **53**, 3442 (2008)
44. A.F. Azevedo, M.R. Baldan, N.G. Ferreira, Int. J. Electrochem. **2012**, 1 (2012)
45. K. Ushizawa, Y. Sato, T. Mitsumori, T. Machinami, T. Ueda, T. Ando, Chem. Phys. Lett. **351**, 105 (2002)
46. J. Zang, Y. Wang, L. Bian, J. Zhang, F. Meng, Y. Zhao, X. Qu, S. Ren, Int. J. Hydrog. Energy **37**, 6349 (2012)
47. C. Wang, J. Chen, G. Yang, N. Xu, Angew. Chem. Int. Edit. **44**, 7414 (2005)
48. P.A Swarthmore, JCPDS International Center for Diffraction Data (1991)
49. R.G. Compton, G.G. Wildgoose, N.V. Rees, I. Streeter, R. Baron, Chem. Phys. Lett. **459**, 1 (2008)
50. M.P.N. Bui, X.H. Pham, K.H. Han, C.A. Li, Y.S. Kim, G.H. Seong, Sens. Actuat. B Chem. **150**, 436 (2010)
51. Y. Han, J. Zheng, S. Dong, Electrochim. Acta **90**, 35 (2013)